A phenomenological model of dynamical arrest of electron transfer in solvents in the glass-transition region

Dmitry V. Matyushov[a)]
Department of Chemistry and Biochemistry and the Center for the Early Events in Photosynthesis, Arizona State University, Tempe, Arizona 85287-1604

(Received 30 August 2004; accepted 2 December 2004; published online 17 February 2005)

A phenomenological model of electron transfer reactions in solvents undergoing glass transition is discussed. The reaction constant cuts off slow polarization modes from the spectrum of nuclear thermal motions active on the observation time scale. The arrest of nuclear solvation in turn affects the reaction activation barrier making it dependent on the rate. The resultant rate constant is sought from a self-consistent equation. The model describes well the sharp change in the solvent Stokes shift of optical lines in the glass-transition region. It is also applied to describe the temperature dependence of primary charge separation and reduction of primary pair in photosynthetic reaction centers. The model shows that a weak dependence of the primary charge separation rate on temperature can be explained by dynamical arrest of nuclear solvation on the picosecond time scale of electron transfer. For reduction of primary pair by cytochrome, the model yields a sharp turnover of the reaction kinetics at the transition temperature when nuclear solvation freezes in. © *2005 American Institute of Physics*. [DOI: 10.1063/1.1851981]

I. INTRODUCTION

The Marcus–Hush picture of electron transfer (ET) activation[1] is based on the transition-state theory. The rate constant is the product of the Boltzmann probability for the system to reach the top of the barrier separating the reactants and products and a frequency factor. For weakly coupled donor and acceptor sites, the reaction flux on the barrier top is controlled by the tunneling rate $V/\hbar$, where V is the electronic mixing of the donor and acceptor. The rate constant of ET becomes

$$k_{\mathrm{ET}} = (V/\hbar)^2 \mathrm{FC}. \tag{1}$$

The classical limit of the Franck–Condon (FC) factor describes activated kinetics with the activation energy E_a

$$\mathrm{FC} \propto e^{-E_a/k_{\mathrm{B}}T}. \tag{2}$$

With increasing V or, alternatively, with slowing down the rate of solvent relaxation, reorientation dynamics of the solvent starts to affect the reaction flux on the barrier top and the reaction appears in the regime of solvent dynamics control.[2] However, slow solvent dynamics does not affect the activation barrier E_a as long as the time of experimental observation $\tau_{\mathrm{ET}}=k_{\mathrm{ET}}^{-1}$ is much longer than the relaxation time of any thermal motion driving ET.

This picture of ET activation may change dramatically when the relaxation time of a nuclear mode coupled to ET is comparable to τ_{ET}. Various nuclear modes contribute both dynamically and thermodynamically to one collective reaction coordinate, the energy gap ΔE between the donor and acceptor electronic states (Fig. 1). The equilibrium distribution of energy gaps (solid line in Fig. 1) is characterized by its average $\langle \Delta E \rangle$ and variance $\sigma^2=\langle \Delta E^2 \rangle - \langle \Delta E \rangle^2$. If higher cumulants of ΔE are insignificant, the distribution is Gaussian and the Boltzmann factor in Eq. (2) is given by the probability of achieving the activated state $\Delta E=0$ with the activation energy

$$\frac{E_a}{k_{\mathrm{B}}T} = \frac{\langle \Delta E \rangle^2}{2\sigma^2}. \tag{3}$$

The equilibrium distribution is produced by an ergodic system visiting all parts of its phase space on the time scale of the experiment. If some of the solvent modes coupled to the transferred electron relax on time scales slower than the time τ_{ET}, these modes appear to be dynamically arrested (frozen) on the experimental observation window and the stationary distribution of donor-acceptor energy gaps (dashed line in Fig. 1) differs from the equilibrium distribution.

The present phenomenological model deals with the effect of slowing solvent modes on the distribution of energy gaps. A rigorous calculation of the ET rates at such conditions would require a complete solution of the dynamic problem with dynamically competing nuclear modes analogous to the Sumi and Marcus model[3] dealing with the dynamics of two nuclear modes. Such a solution is presently hard to achieve in view of a broad spectrum of time scales characteristic of a soft condensed solvent undergoing glass transition.[4] The purpose of this study is to present a simple solution which would address the temperature dependence of the activation energy E_a in Eq. (2) resulting from dynamical arrest of nuclear solvation.

A phenomenological model of ET in solvents close to their glass transition has previously been proposed by Hoffman and Ratner (HR).[5] In the HR model the solvent reorganization energy λ_s is *assumed* to follow the Vogel–Fulcher temperature law above the glass-transition temperature T_g,

a)Electronic mail: dmitrym@asu.edu

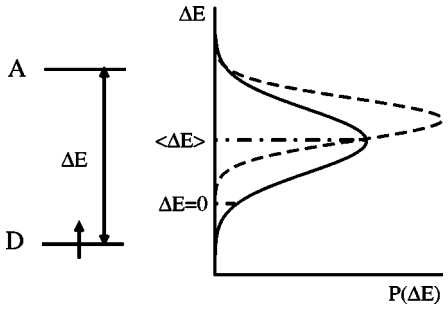

FIG. 1. Distribution of donor-acceptor energy gaps.

$$\lambda_s = \lambda_0 f_{\mathrm{VF}}(T), \tag{4}$$

where

$$f_{\mathrm{VF}}(T) = \exp\left[\frac{D}{T - T_0}\right], \tag{5}$$

and T_0 is the Vogel–Fulcher temperature. According to experimental observations, $T_0/T_g < 1$. What is missing from the HR description is the dynamic nature of the solvent effect on the activation barrier. Indeed, the temperature at which a particular solvent mode freezes in is determined by the competition of its relaxation time $\tau(T)$ with τ_{ET}. The time τ_{ET} is in turn affected by that mode freezing through the alteration of the stationary distribution $P(\Delta E)$ (Fig. 1). The ET rate constant then follows from a self-consistent relation which should be solved at each temperature. In what follows we formulate such a procedure and consider its implications for the ET kinetics.

II. MODEL

Consider an electronic transition within a donor-acceptor complex immersed in a condensed solvent such that the Hamiltonian of the whole system in the initial $(i=1)$ and the final $(i=2)$ states can be written as follows:

$$H_i = I_i + H_i^q + H_i^s. \tag{6}$$

The Hamiltonian H_i^q describes nondissipative vibrations of the solute and phonons of the solvent and I_i is the gas-phase energy of the donor-acceptor complex. The low-frequency, dissipative motions of the solvent are described by the Hamiltonian H_i^s. The solvent can refer to a liquid solvent for solution redox reactions or to protein and water combined in biological applications. In the present formulation, the classical solvent mode undergoes glass transition before quantum effects gain importance, thus classical description is adopted for H_i^s.

Following the traditional prescription of the Marcus model,[1] solvent nuclear polarization is a classical, overdamped collective mode coupled to ET. The macroscopic dynamics of the solvent polarization is determined by the frequency-dependent dielectric constant $\epsilon(\omega)$. Once the solvent is cooled down, the characteristic relaxation time of polarization fluctuations grows according to the Vogel–Fulcher law until it becomes comparable to the ET rate. At this point, each donor-acceptor complex senses its particular microscopic environment characterized by the relaxation time $\tau(T)$.[6] This spatially heterogeneous distribution of relaxation times leads to deviations of the dielectric function $\epsilon(\omega)$ from the single-exponential Debye expression. The experimental relaxation spectra are commonly described by the empirical Havriliak–Negami equation[4]

$$\epsilon(\omega) = \epsilon_\infty + \frac{\Delta\epsilon}{[1 + (i\omega\tau_{CD})^{1-\alpha}]^\gamma}, \tag{7}$$

where ϵ_∞ is the optical dielectric constant, $\Delta\epsilon = \epsilon_s - \epsilon_\infty$, and ϵ_s is the static dielectric constant. The empirical dielectric constant follows from the Debye law by integrating the Debye equation with the distribution of relaxation times $g(\tau)$:[7]

$$\epsilon(\omega) = \int g(\tau)\epsilon^D(\omega,\tau)d\tau, \tag{8}$$

where

$$\epsilon^D(\omega,\tau) = \epsilon_\infty + \Delta\epsilon(1 + i\omega\tau)^{-1}. \tag{9}$$

Once the temperature falls below T_g, each donor-acceptor complex with its microscopic solvent environment gets trapped in a particular valley of the rugged energy landscape.[8] The distribution of activation energies of ET is then characterized by static heterogeneity which, in principle, depends on the cooling rate. The slowing down of the dielectric relaxation time when approaching the glass-transition temperature T_g is the principal reason for the dynamical arrest and pronounced temperature dependence of nuclear solvation which, in turn, is projected into a non-Arrhenius temperature dependence of the rate constant.

A. ET rate

Within the Condon approximation, the FC factor in Eq. (1) reads

$$\mathrm{FC} = \int_{-\infty}^{\infty} \langle e^{-iH_1 t/\hbar} e^{iH_2 t/\hbar}\rangle_1 dt, \tag{10}$$

where $\langle\cdots\rangle_1$ denote ensemble average over the initial state with $i=1$. If the dissipative solvent mode is decoupled from the vibrational modes, the above expression can be rewritten in terms of generating functionals for each mode

$$\mathrm{FC} = \int_{-\infty}^{\infty} \frac{d\omega}{2\pi} \mathcal{G}_q(\omega_{\mathrm{tr}} - \omega)\mathcal{G}_s(\omega). \tag{11}$$

Here, the generating functional for mode $X = q, s$

$$\mathcal{G}_X(\omega) = \int_{-\infty}^{\infty} \exp[i\omega t - g_X(t)]dt \tag{12}$$

is given in terms of the broadening function $g_X(t)$ (Refs. 9 and 10)

$$g_X(t) = \frac{1}{\pi}\int_0^\infty \frac{d\omega}{\omega^2}(1-\cos\omega t)\chi_X''(\omega)\coth\frac{\beta\hbar\omega}{2} + \frac{i}{\pi}\int_0^\infty \frac{d\omega}{\omega^2}(\omega t - \sin\omega t)\chi_X''(\omega), \tag{13}$$

where $\beta=1/k_BT$ and $\chi_X''(\omega)$ is the spectral density corresponding to the nuclear coordinate X.

In Eq. (11),

$$\hbar\omega_{tr} = \Delta G + \lambda_q + \lambda_s \tag{14}$$

is the condensed-phase vertical transition energy between the initial and final ET states. The equilibrium energy gap ΔG can be split into the difference of free energies of nuclear solvation (subscript "*n*") ΔG_n and the nonpolar gap (subscript "np") ΔE_{np}:

$$\Delta G = \Delta E_{np} + \Delta G_n. \tag{15}$$

The nonpolar gap is composed of the gas-phase 0-0 transition energy $\Delta I=I_2-I_1$ and a contribution from electronic solvation. The latter is made by the free energy of solvation by induced dipoles, ΔG_e (induction forces) and the energy of dispersion solvation. Finally, λ_q and λ_s in Eq. (14) stand for the reorganization energies of, correspondingly, the vibrational and solvent modes.

If q is an optical phonon with the frequency ω_q, the spectral density becomes[10]

$$\chi_q''(\omega) = \pi\omega_q^2 S_q[\delta(\omega-\omega_q) - \delta(\omega+\omega_q)], \tag{16}$$

where $S_q=\lambda_q/\hbar\omega_q$ is the Huang–Rhys factor. The vibronic generating functional in Eq. (11) is then a weighted sum over the vibronic transitions with frequencies $\omega_{tr}-S_q\omega_q+l\omega_q$ (Refs. 10 and 11)

$$\mathcal{G}_q(\omega_{tr}-\omega) = 2\pi\sum_{l=-\infty}^{\infty} A_l\delta(\omega_{tr}-S_q\omega_q+l\omega_q-\omega), \tag{17}$$

where

$$A_l = \exp[-S_q\coth\beta\hbar\omega_q/2 + l\beta\hbar\omega_q/2]I_l\left(\frac{S_q}{\sinh\beta\hbar\omega_q/2}\right) \tag{18}$$

and $I_l(x)$ is the modified Bessel function.

Several effects contribute to the deviation of the spectral density from the simple form given in Eq. (16). Apart from the fact that a distribution of phonon frequencies should be considered in realistic modeling,[12] homogeneous broadening, vibrational decoherence, and static heterogeneity all contribute to the broadening of the δ-function distribution. Accurate description of low-temperature line shapes requires asymmetric broadening functions.[13] For simplicity, we consider here a temperature independent Gaussian broadening with the width Γ responsible for static heterogeneity of the frozen solvent. This replaces Eq. (17) with a weighted sum of Gaussians

$$\mathcal{G}_q(\omega_{tr}-\omega) = (\sqrt{2\pi}\hbar/\Gamma)\sum_{l=-\infty}^{\infty} A_l\exp[-\hbar^2(\omega_{tr}-S_q\omega_q+l\omega_q-\omega)^2/2\Gamma^2]. \tag{19}$$

B. Classical mode

When solvent polarization is given by a classical Gaussian field, the corresponding generating functional is a Gaussian function

$$\mathcal{G}_s(\omega) = (\sqrt{2\pi}\hbar/\sigma_s)\exp\left[-\frac{(\hbar\omega)^2}{2\sigma_s^2}\right], \tag{20}$$

where

$$\sigma_s^2 = 2k_BT\lambda_s. \tag{21}$$

Both the solvent reorganization energy λ_s and the nuclear component of the free energy gap ΔG_n are produced by polarization modes relaxing faster than the rate of ET. This fact can be accommodated in terms of the inverted-space response function

$$\boldsymbol{\alpha}(\mathbf{k}) = \frac{1}{\pi}\int_{k_{ET}}^{\omega_c}\frac{d\omega}{\omega}\boldsymbol{\chi}''(\mathbf{k},\omega). \tag{22}$$

Here, the two-rank tensor $\boldsymbol{\chi}(\mathbf{k},\omega)$ is the linear response function of the solvent nuclear polarization to the electric field of the donor-acceptor complex immersed into the solvent. Further, ω_c denotes an upper-bound frequency of the classical dielectric spectrum and k_{ET} puts the lower limit to the spectrum of frequencies active in driving ET.

A full microscopic description of the problem requires knowledge of the microscopic, k-dependent response function.[14] We, however, resort here to a simplified formulation assuming dielectric continuum response in which case the dependence on k is neglected, $\boldsymbol{\chi}''(\mathbf{k},\omega)\simeq\boldsymbol{\chi}''(0,\omega)$. The longitudinal projection $\chi^L(\mathbf{k},\omega)=\mathbf{k}\cdot\boldsymbol{\chi}''(\mathbf{k},\omega)\cdot\mathbf{k}$ dominates the polar solvent response for long-range ET.[14] The continuum response function is then fully determined by the frequency-dependent dielectric constant of the solvent

$$\chi^L(0,\omega) = \frac{1}{4\pi}\frac{\epsilon''(\omega)}{|\epsilon(\omega)|^2}. \tag{23}$$

With this definition of the solvent response function, λ_s and ΔG_n are given by the following relations:

$$\lambda_s(k_{ET}) = \lambda_0 f(k_{ET}) \tag{24}$$

and

$$\Delta G_n(k_{ET}) = \Delta G_0 f(k_{ET}). \tag{25}$$

Here λ_0 and ΔG_0 are the full thermodynamic values for the reorganization energy and solvation free energy which both are determined by the complete spectrum of the polarization fluctuations. The function $f(k_{ET})$ incorporates the cutoff of the spectrum of polarization fluctuations due to dynamical arrest of polarization modes which are slow compared to the reaction rate:

$$f(k_{\rm ET}) = \int_{k_{\rm ET}}^{\omega_c} \frac{d\omega}{\omega} \frac{\epsilon''(\omega)}{|\epsilon(\omega)|^2} \Bigg/ \int_0^{\omega_c} \frac{d\omega}{\omega} \frac{\epsilon''(\omega)}{|\epsilon(\omega)|^2}. \tag{26}$$

In the case of Debye dielectric relaxation [Eq. (9)] the function $f(k_{\rm ET})$ becomes ($\omega_c \gg \tau_{\rm L}^{-1}$)

$$f(k_{\rm ET}) = (2/\pi)\tan^{-1}[1/k_{\rm ET}\tau_{\rm L}(T)]. \tag{27}$$

Here, $\tau_{\rm L}(T)$ is the longitudinal relaxation time which depends on temperature according to the Vogel–Fulcher law

$$\tau_{\rm L}(T) = \tau_{\rm L}^0 f_{\rm VF}(T). \tag{28}$$

Solvent response in proteins is highly heterogeneous with spatially distributed relaxation times. Equation (24) can be generalized to accommodate this fact in an additive form

$$\lambda_s(k_{\rm ET})/\lambda_0 = \sum_j \theta_j f_j(k_{\rm ET}). \tag{29}$$

Here, $\theta_j = \lambda_{0j}/\lambda_0$ is the fraction of mode j in the total solvent reorganization energy and

$$f_j(k_{\rm ET}) = (2/\pi)\tan^{-1}[1/k_{\rm ET}\tau_{Lj}(T)]. \tag{30}$$

The additive approximation of Eq. (29) is based on the assumption of statistical independence of k-space polarization fluctuations corresponding to different modes: $\langle \delta\mathbf{P}_i(\mathbf{k})\delta\mathbf{P}_j(\mathbf{k}')\rangle = 0$ when $i \neq j$. It is expected to apply to polarization modes reflecting drastically different length scales, e.g., bulk polarization vs polarization due to protein's polar/charged side groups.

The free energy of nuclear solvation is affected by the spectrum of polarization modes still active on the time scale of ET through the cutoff function $f(k_{\rm ET})$. The solvation energy in turn affects the stationary distribution of donor-acceptor energy gaps entering the rate constant [Eqs. (2) and (3)]. The resultant rate constant should be sought from a self-consistent equation. Combining the generating functionals for vibrational and polarization modes in Eqs. (11), (19), and (20) one gets

$$k_{\rm ET}^{\tau} = \frac{V^2}{\hbar}\left(\frac{2\pi}{\Gamma^2 + \sigma_s^2(k_{\rm ET}^{\tau})}\right)^{1/2} \times \sum_{l=-\infty}^{\infty} A_l \exp\left[-\frac{(\Delta E_{\rm np} + (\Delta G_n + \lambda_s) f(k_{\rm ET}^{\tau}) + l\hbar\omega_q)^2}{2(\Gamma^2 + \sigma_s^2(k_{\rm ET}^{\tau}))}\right], \tag{31}$$

where

$$\sigma_s(k_{\rm ET}^{\tau}) = 2k_{\rm B}T\lambda_s(k_{\rm ET}^{\tau}). \tag{32}$$

The superscript "τ" for the ET rate constant in Eq. (31) indicates that the self-consistent equation is solved for a specific donor-acceptor complex coupled to a local solvent environment relaxing with the relaxation time $\tau(T)$. The corresponding response function is then of the Debye type, and the cutoff function is given by Eq. (27). For experiments reflecting ensemble average over donor-acceptor complexes, the observed decay of the donor population $P_D(t)$ is nonexponential as a result of averaging over the distribution of relaxation times $g(\tau)$ and static heterogeneity, $\langle\cdots\rangle_{\rm het}$:

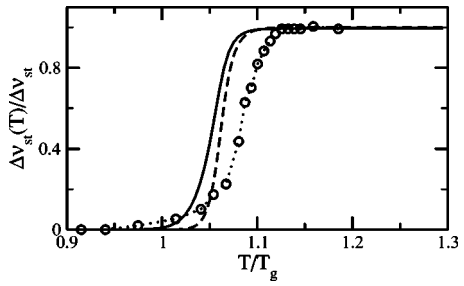

FIG. 2. Temperature variation of the solvent Stokes shift for quinoxaline in MTHF. The solid line refers to the calculation according to Eqs. (34) and (35), the dashed line is Eq. (34) with Debye single-exponential relaxation, and points refer to experiment (Ref. 15). The calculation parameters are $T_g = 90.7$ K, $\alpha = 0$, $\gamma = 0.48$, $\epsilon_\infty \simeq 3$, $\epsilon_s \simeq 19$ [Eq. (7)] (Ref. 15) $D = 792.5$ K, $T_0 = 71.7$ K, and $\tau_{\rm CD}^0 = 1.27 \times 10^{-16}$ s [Eqs. (7) and (28)] (Ref. 16). The dotted line connects the experimental points.

$$P_D(t) = \int \langle e^{-k_{\rm ET}^{\tau} t}\rangle_{\rm het} g(\tau) d\tau. \tag{33}$$

III. SPECTROSCOPIC EXPERIMENT

Spectroscopic measurements of the solvent Stokes shift of optical lines provide direct evidence of the sharp dependence of the solvent reorganization energy on temperature in the glass-transition region.[15] The spectroscopic experiment also offers a significant simplification of the problem since the relaxation window is fixed by the experimental apparatus at the observation time $\tau_{\rm obs}$. The drop of the solvent Stokes shift with decreasing temperature is thus a kinetic effect arising from the competition of the observation time and solvent relaxation time at low temperatures. The solvent reorganization energy $\lambda_s(T)$ relative to its high-temperature value λ_0 then follows from Eqs. (24) and (27):

$$\lambda(T)/\lambda_0 = (2/\pi)\int g(\tau)\tan^{-1}[\tau_{\rm obs}/\tau_{\rm L}(T)]d\tau. \tag{34}$$

Figure 2 shows the comparison of Eq. (34) (lines) to low-temperature measurements (points) of the solvent Stokes shift for the quinoxaline dye in 2-methyltetrahydrofurane (MTHF) near the glass-transition temperature $T_g = 90.7$ K. The recording time window is $\tau_{\rm obs} = 1$-2 ms.[15,16] Independent dielectric measurements for MTHF in the same temperature range have been fitted[15] to Eq. (7) with the exponents $\alpha = 0$ and $\gamma = 0.48$, dielectric constants $\epsilon_\infty \simeq 3$ and $\epsilon_s \simeq 19$, and the Vogel–Fulcher relaxation time $\tau_{\rm CD}$ in Eq. (7) with $D = 792.5$ K, $T_0 = 71.7$ K, and $\tau_{\rm CD}^0 = 1.27 \times 10^{-16}$ s.[16] This Cole–Davidson form of the dielectric function ($\alpha = 0$) allows an analytical representation for the distribution of relaxation times $g(\tau)$ in the form[7]

$$g(\tau) = \theta(\tau_{\rm CD} - \tau)\frac{\sin(\pi\gamma)}{\pi\tau}\left(\frac{\tau}{\tau_{\rm CD} - \tau}\right)^{\gamma}, \tag{35}$$

where $\theta(x)$ is a step function: $\theta(x) = 1$ at $x > 0$ and $\theta(x) = 0$ at $x \leqslant 0$. Calculations with Eqs. (34) and (35) are shown by the solid line in Fig. 2. The Debye relaxation corresponding to $g(\tau) = \delta(\tau - \tau_{\rm CD})$ is shown by the broken line. Although there is no exact match between experimental data and Eqs. (34) and (35), a stepwise increase of the reorganization energy is

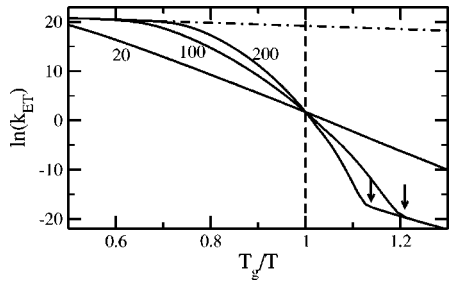

FIG. 3. Rate constant of charge separation, $\langle \Delta E \rangle = \Delta E_{\rm np}$, at different solvent fragilities (indicated on the plot). The dash-dotted line shows the rate when dynamical arrest is neglected, $f(k_{\rm ET})=1$. The vertical arrows indicate the chemical temperature $T_{\rm chm}$ at which activation by nuclear modes freezes in. The calculations are done according to Eq. (31) with the parameters $V=10$ cm^{-1}, $\lambda_s=1$ eV, $\Delta G_n=-\lambda_s$, $\Delta E_{\rm np}=0.5$ eV, $\lambda_q=1500$ cm^{-1}, $\hbar\omega_q=1500$ cm^{-1}, and $\Gamma=120$ cm^{-1}. The solvent relaxation is modeled with $T_g=200$ K and $\tau_0=10^{-16}$ s such that at $T/T_g=2$ the longitudinal relaxation time is $\tau_{\rm L}\simeq 10^{-13}$ s at $m=200$ and $\tau_{\rm L}\simeq 10^{-9}$ s at $m=20$.

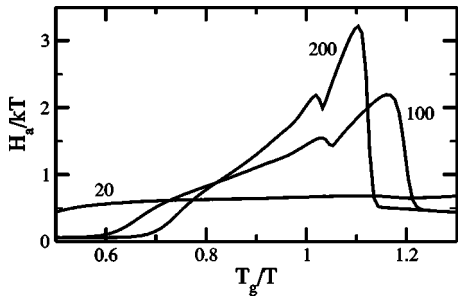

FIG. 4. Enthalpy of activation [Eq. (37)] vs T_g/T for solvents with varying fragility (indicated on the plot). The calculation parameters are the same as in Fig. 3.

qualitatively reproduced by the present model. The too steep rise of $\lambda_s(T)$ with temperature is likely related to too fast dynamics predicted by the dielectric response in low-temperature solvents.[17] A full k dependence of the polarization response function is required for a more quantitative description. Freezing of orientational polarization may occur gradually between the solvation layers of an optical dye.[18] The gradual freezing should result in a weaker dependence of the Stokes shift on temperature compared to any model that does not incorporate heterogeneous orientational dynamics of solvation layers.

IV. ET RATE CONSTANT

The calculation of the solvent reorganization energy in the preceding section shows that λ_s is not strongly affected by heterogeneous distribution of relaxation times. Therefore, the numerical examples in this section refer to a site specific rate constant $k_{\rm ET}=k_{\rm ET}^{\tau}$ or, alternatively, to the assumption $g(\tau)=\delta(\tau-\tau_{\rm CD})$.

The alteration of the relaxation time in the glass-transition region can be characterized by the Vogel–Fulcher strength parameter D in Eq. (5) or, alternatively, by the fragility parameter[4]

$$m = \left. \frac{d \log_{10}\tau(T)}{d(T_g/T)} \right|_{T=T_g}. \tag{36}$$

The fragility parameter determines the temperature range in which the relaxation time changes substantially: this range shrinks with increasing m. Correspondingly, for a fixed experimental temperature range, the dynamical arrest manifests itself more dramatically in the form of deviation of dynamic properties from the Arrhenius law when m increases. This feature is indeed seen in Fig. 3 where the rate constant of a model charge separation reaction with $\Delta G_n=-\lambda_s$ is plotted against T_g/T for solvents with increasing fragility. The dash-dotted line refers to the traditional Marcus–Hush description with λ_s independent of temperature.

Dynamical arrest of nuclear polarization modes driving ET is a kinetic phenomenon which is affected by both the relaxation time of the solvent and the rate of ET. The temperature at which such an arrest occurs is higher than the fictive temperature of structural arrest of the solvent, but can fall either above or below the glass-transition temperature T_g which is rather arbitrary defined.[4] Dynamical arrest is marked by a sharp drop of $f(k_{\rm ET})$ from $f(k_{\rm ET})\simeq 1$ to $f(k_{\rm ET}) \ll 1$. The temperature at which $\lambda_0 f(k_{\rm ET})$ becomes much smaller than any energy scale affecting the ET rate can be identified as the "chemical fictive temperature" or "chemical reaction freezing temperature" $T_{\rm chm}$ introduced by Angell.[4,19] This temperature (shown by vertical arrows in Fig. 3) marks the onset of freezing of nuclear fluctuations driving the reaction over the activation barrier in the classical transition-state theory. Below $T_{\rm chm}$ a reaction can be activated by coupling to localized (skeletal vibrations) and delocalized (phonons) vibrations of the solute and the solid solvent.

Figure 3 shows that $T_{\rm chm}$ decreases with slowing the polarization fluctuations, i.e., dynamical arrest occurs at lower temperatures for slower polarization modes. This observation suggests that the temperature variation of the rate constant may be quite complex for systems characterized by a hierarchy of relaxation times. The dependence $\ln(k_{\rm ET})$ vs $1/T$ may pass through several sequential dips, each corresponding to freezing of a particular polarization mode. The chemical fictive temperature in fragile solvents can be identified with a maximum of the reaction enthalpy defined as

$$H_a = -\frac{\partial \ln k_{\rm ET}}{\partial \beta} \tag{37}$$

at $T_{\rm chm}$ (Fig. 4).

Figures 3 and 4 refer to the case of charge separation from a nonpolar state of the donor-acceptor complex when the effect of nuclear solvation manifests itself only in the variance σ_s^2 in Eq. (31). When $\Delta G_n+\lambda_s\neq 0$, the picture becomes more complex due to a strong dependence on temperature for both $\langle \Delta E \rangle$ and σ_s^2 near $T_{\rm chm}$. A particularly sharp dependence on temperature is achieved when the low-temperature and high-temperature ET kinetics fall in different regions of ET, normal and inverted. Figure 5 illustrates this notion by showing the temperature dependence of the rate constant for a model charge shift reaction with $\Delta G_n=0$ and $\Delta E_{\rm np}<0$. The unfreezing of the nuclear reorganization energy then leads to a positive shift of $\langle \Delta E \rangle$ from $\langle \Delta E \rangle = E_{\rm np}<0$ through the activationless transition at $\langle \Delta E \rangle = 0$ back to the activated kinetics with $\langle \Delta E \rangle = E_{\rm np}+\lambda_0>0$.

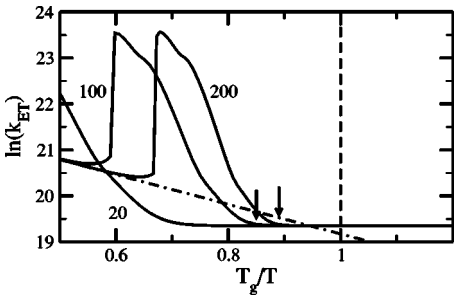

FIG. 5. Rate constant for charge shift with $\Delta G_n=0$ and $\Delta E_{\rm np}=-0.5$ eV. All other parameters and notation are as in Fig. 3.

The ET rate in Fig. 5 is very weakly temperature dependent at low temperatures since the reaction is in the inverted region where the rate is fully determined by nuclear tunneling of vibrational modes. Nuclear solvation starts affecting ET dynamics at $T \geqslant T_{\rm chm}$. For fast reactions, $T_{\rm chm}$ can be substantially higher than T_g. This pattern is characteristic of primary charge separation in photosynthetic systems where $T_{\rm chm}$ is above the physiological range of temperatures and electronic transitions are driven by optical phonons of the low-temperature solid solvent and by skeletal vibrations of the solute (see below).

A. Primary charge separation in photosynthetic reaction centers

Primary charge separation in bacterial reaction centers is among the fastest processes on the biological time scale. Yet the kinetics is extremely robust with the ET time of 3.5 ps at room temperature accelerating to 1.2 ps at 8 K.[20] The mechanism of primary charge separation has been intensely debated in particular focusing on sequential vs direct ET between the photoexcited primary pair P^* and bacteriopheophytin $H_{\rm L}$.[21,22] The controversy has mostly originated from the unsettled value of the equilibrium Gibbs energy of the accessory bacteriochlorophyll $B_{\rm L}$ which is the intermediate state in the sequential mechanism. Most recent measurements place the equilibrium energy of $B_{\rm L}$ about 0.04 eV below P^* thus favoring the sequential mechanism.[23]

Traditional theories of radiationless transitions require the reaction to be on the top of the Marcus inverted parabola, $\hbar\omega_{\rm tr}=\Delta G+\lambda_s+\lambda_q \simeq 0$, in order to achieve weak temperature dependence of the ET rate observed in the experiment. Therefore, in addition to the equilibrium free energy gap ΔG, one needs the reorganization energies λ_q and λ_s. The former is relatively well established from the combination of low-temperature hole burning,[13] Raman spectroscopy,[24] and Molecular Dynamics (MD) simulations.[12] The latter has recently become available from kinetic measurements on a series of reaction center mutants of *Rhodobacter sphaeroides*.[25–28] The first estimate by Bixon *et al.*[21] based on early mutagenesis results[25–27] gave $\lambda_s \simeq 0.1$ eV and $\Delta G=-0.06$ eV. A more recent study[28] using an extended list of mutants with their midpoint potentials below wild type has lead to a surprising value of $\lambda_s \simeq 0.18$ eV at $\Delta G \simeq -0.06$ eV. These two values place the wild type reaction center about 0.1 eV below the maximum of Marcus parabola. With these ΔG and λ_s the standard theories predict many orders of magnitude change in ET rates when going from room to cryogenic temperatures. Note that the value $\lambda_s \simeq 0.15-0.25$ eV close to the estimate by Haffa *et al.*[28] has been recently obtained from very extensive MD simulations of the wild type reaction center.[29]

The apparent contradiction between low-temperature kinetic measurements[20] and high-temperature mutagenesis data[28] indicates that either some assumptions of the traditional kinetic analysis of ET rates are not met by photosynthetic primary charge separation (e.g., some nuclear modes are not equilibrated on the reaction time scale[30]) or nuclear solvation, reflected by the equilibrium energy gap, somehow does not affect the reaction rate. The present analysis supports the second notion. Our principle result is that nuclear solvation can be dynamically arrested in the whole experimentally studied temperature range due to the fast rate of primary charge separation. When the function $f(k_{\rm ET})$ is close to zero, both nuclear solvation parameters, ΔG_n and λ_s, can be dropped from the equation for the ET rate constant. The nuclear solvation energy thus does not appear in the reaction free energy and the ET energy gap law should consider $\ln(k_{\rm ET})$ vs $\Delta E_{\rm np}$ instead of ΔG. Consequently, the analysis based on the dependence of the ET rate on free energy gaps obtained from *equilibrium, high-temperature* midpoint potentials cannot provide an estimate of λ_s and its magnitude still remains an open question. Note that relatively long simulation runs reported in Ref. 29 give an estimate of the thermodynamic reorganization energy λ_0.

Other parameters entering the ET rate are frequencies and couplings of nuclear vibrations, low-temperature static inhomogeneity, and longitudinal relaxation times of classical nuclear modes. The frequencies and couplings of vibrations of cofactors and the protein matrix have been extensively studied by hole burning,[13] time-resolved stimulated emission,[34] resonant Raman spectroscopy,[24] and MD simulations.[12] A compilation of parameters used in one-mode calculations is listed in Table I.

Specifying the longitudinal relaxation time requires knowledge of the microscopic mechanism of polarization fluctuations. An obvious assumption is that bulk water is responsible for nuclear polarization. The dielectric relaxation of water is well documented at high temperatures and a Vogel–Fulcher fit was suggested into the supercooled region[35] based on dielectric measurements in nanoscale pores[36] and diffusivity data:[37] $D=898$ K, $\tau_{\rm L}^0=[\epsilon_\infty/\epsilon_s(T)] \times 5.95\times 10^{-14}$ s, $T_0=118$ K. When these parameters are used for primary charge separation along with $\lambda_0=0.18$ eV,[29] $\epsilon_\infty=5$ (fit of the low-frequency dielectric measurements[38]), and $\epsilon_s(T)$ from Ref. 38, the ET rate drops significantly at $T>210$ K in contrast to the flat temperature dependence seen in experiment.[20] Therefore, preserving dynamical arrest of nuclear solvation at $T \simeq 300$ K requires either a substantial decrease of the thermodynamic reorganization energy λ_0 or much slower polarization dynamics. Several factors may contribute to slower longitudinal dynamics of water: (i) lower ϵ_s in the vicinity of the protein, (ii) slower dielectric relaxation of hydration layers on the protein surface, and (iii) slower dynamics due to solvent's confinement. However, all these effects can hardly account for the longitudinal relax-

TABLE I. Parameter values for calculations. Calculations for primary charge separation in *Rhodobacter sphaeroides* and charge shift in *Chromatium* are done with $\theta_W=0$ and $\theta_W=1$ [Eq. (38)], respectively.

System	Γ cm^{-1}	ω cm^{-1}	S	V cm^{-1}	λ eV	ΔE_{np} eV	ΔG eV
Rhodobacter sphaeroides	120[a]	95[b]	5.8[c]	29[d]	0.18[e]	−0.012	−0.06[e]
Chromatium	120[a]	95[b]	5.8[c]	1.6[f]	1.0[f]	0.0[g]	−0.16[f]

[a]From Ref. 31.
[b]From Ref. 21.
[c]Based on the reorganization energy 553 cm^{-1} reported in Ref. 30.
[d]From the fit the experimental energy gap law given in Fig. 6. Similar values are reported in Refs. 20, 21, and 31.
[e]From Ref. 28.
[f]From Ref. 32.
[g]Adopted based on the equilibrium constant $\simeq 0.25$ at 140 K (Ref. 33).

ation time of the order of 100–200 ps at $T\simeq 300$ K which is required for dynamical arrest. The rotational relaxation time of water in hydration layers is of the order of 40 ps,[39] which reduces further when multiplied with $\epsilon_\infty/\epsilon_s$. Tightly bound water may fall in the nanosecond relaxation range, but its intensity in the dielectric response is very weak.[39] The effect of solvent confinement relaxation is pronounced at low temperatures close to the glass transition, but is less important at room temperature.[40] On the other hand, dipolar fluctuations of the protein are dominated by charged side chains which contribute to the dielectric spectrum at 100–800 ps.[41–44] A single layer of water is sufficient to allow side chain motions which are highly damped by the solvent.[45]

Side chain rotations lack the cooperativity of the primary α relaxation and the relaxation time obeys the Arrhenius law. This secondary β-relaxation becomes active at temperatures as low as 150 K when the onset of motional freedom is seen as a gradual increase in protein's heat capacity[46] and an increase of the Debye–Waller factor in neutron scattering.[47] This temperature also marks the onset of activated kinetics of charge shift reactions in many photosynthetic bacteria[48] and photosystem I.[49] Based on the analysis of temperature dependent ET rates, Hales suggested[48] that freezing of side chain rotations is responsible for the change in the reaction temperature dependence. Therefore, according to this view, thermal motion of side chains activate ET at high temperatures. This suggestion certainly requires a more careful study. At present, the actual splitting of the reorganization energy between components originating from coupling to water and to polar/charged side chains is unknown. Note, however, that, in contrast to electrolyte solutions, charged side chains do not form Hückel screening of ionic fields and their mobility may strongly affect electronic levels of cofactors buried inside the protein.

Time-resolved measurements of solvation dynamics also point to slow dynamics of optical chromophores located in protein's hydrophobic environment. Fluorescence dynamics of optically excited tryptophan buried inside a protein was reported in the 100 ps range.[50] Recent measurements of the Stokes shift dynamics of Zn(II)-substituted cytochrome *c* have shown an approximately equal splitting of the Stokes shift between the protein matrix relaxing on the time scale of 250 ps and much slower side chains relaxing on the time scale of 1500 ps.[51] On the other hand, the use of optical probes partially exposed to the solvent indicates the existence of fast (<100 fs) inertial dynamics correlated with motions of the bulk aqueous solvent.[52,53] The dynamics of the response is thus strongly dependent on the locations of the donor and acceptor sites in the protein.[54] The photosynthetic cofactors are located inside the hydrophobic protein core, and solvation dynamics obtained on the porphyrin probe[51] seems to be more relevant to this situation. The separation of the nuclear polarization response into the components originating from side chain rotations and the protein matrix is currently hard to assert, and we will tentatively attribute the slow dynamics to side chain fluctuations.

For the present modeling we will assume the two-mode form of Eq. (29)

$$\lambda(k_{ET})/\lambda_0 = (1-\theta_W)f_{SC}(k_{ET}) + \theta_W f_W(k_{ET}), \tag{38}$$

where θ_W is the fraction of reorganization energy from bulk water. The functions $f_W(k_{ET})$ and $f_{SC}(k_{ET})$ refer to water and side chain relaxation, respectively. The relaxation time for the latter is taken from low-frequency mechanical relaxation measurements of lysozyme yielding the activation energy of 75 kJ/mol (Ref. 55) with the preexponential factor calculated from the temperature 157 K marking the onset of β relaxation as seen by protein calorimetry:[46]

$$\tau_{SC}(T) = 1.3\times 10^{-21} e^{9000/T}, \tag{39}$$

where T is in K and τ_{SC} is in s.

The only two parameters left to be specified are the electronic coupling V and the nonpolar energy gap ΔE_{np}. These are obtained by fitting the energy gap law from recent mutagenesis data.[28] Mutations of the primary pair used to study the ET energy gap law alter the chemical identity of the ET donor thus affecting the magnitude of ΔE_{np}. This is the relevant energy gap for the dynamically frozen regime of ET. If one assumes that the energy of the ground state of the primary pair remains unchanged by mutations (electrostatic mutations), one can estimate the change in ΔE_{np} from the change in the absorption energy of the primary pair relative to that of the wild type (superscript "Wt") reaction center:[28] $\hbar\Delta\omega_{abs}=\Delta E_{np}-\Delta E_{np}^{Wt}$.

In Fig. 6 a fit of experimental reaction rates is shown with V and ΔE_{np}^{Wt} considered as fitting parameters. The solvent dynamics is assumed to be completely due to β relaxation of protein's side chains [$\theta_W=0$ in Eq. (38)]. The fit

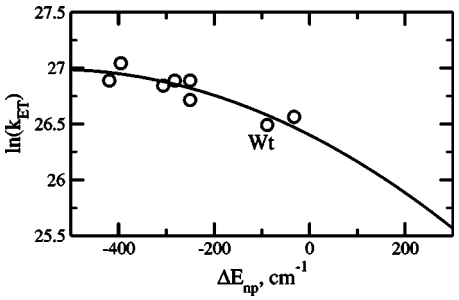

FIG. 6. k_{ET} vs ΔE_{np} for a series of mutants from Ref. 28 (points, $T=295$ K). The energy gap ΔE_{np} is calculated from the gap for the wild type reaction center ΔE_{np}^{Wt}, and the shift in the absorption energy of mutated primary pairs (Ref. 28). ΔE_{np}^{Wt} and V are considered as fitting parameters with the best fit values $\Delta E_{np}^{Wt}=93$ cm^{-1} and $V=29$ cm^{-1}. Other calculation parameters are listed in Table I, $\theta_W=0$. The wild type reaction center is labeled as "Wt."

yields $V=29$ cm^{-1}, which compares very well with commonly reported values,[20,21,31] and $\Delta E_{np}^{Wt}=-93$ cm^{-1}. The latter value does not reproduce the observed temperature dependence of the ET rate if ΔE_{np}^{Wt} is assumed to be temperature independent (Fig. 7). A downward shift of ΔE_{np}^{Wt} to about -400 cm^{-1} is required to bring the reaction in the nearly activationless region when the rate starts to drop with temperature due to a decrease in the population of a resonant vibronic state responsible for nuclear tunneling. There is, however, a good reason to believe that ΔE_{np}^{Wt} is sufficiently temperature dependent to explain experimental ET rates.

The nonpolar energy gap ΔE_{np}^{Wt} includes a gas-phase component and instantaneous solvation by electronic degrees of freedom of the protein matrix and water. Electronic solvation, insensitive to dynamical arrest of overdamped nuclear modes, includes two contributions: from dispersion forces and from induction forces. The former most likely does not change dramatically with electronic transition and does not affect the difference ΔE_{np}^{Wt}. Solvation by induced dipoles is, however, a bilinear functional of the electric field of the donor-acceptor complex in the initial $\mathbf{E}_1(\mathbf{r})$ and final $\mathbf{E}_2(\mathbf{r})$ states. Induction solvation should, therefore, change substantially when the large dipole moment ($\simeq 51$ D) is developed upon primary charge separation.

When polarizable groups carrying the average polarizability α are distributed around the donor-acceptor complex

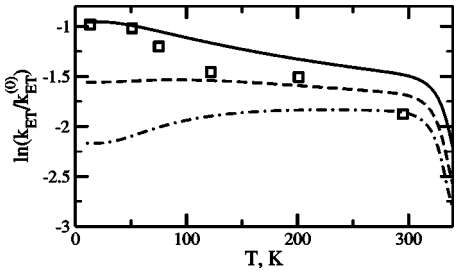

FIG. 7. $k_{ET}/k_{ET}^{(0)}$ vs T at $\Delta E_{np}=-400$ cm^{-1} (solid line), $\Delta E_{np}=-200$ cm^{-1} (dashed line), and $\Delta E_{np}=-93$ cm^{-1} (dash-dotted line). For the calculation of the longitudinal relaxation time, $\theta_W=0$ is used in Eq. (38) with other parameters listed in Table I. Squares indicate experimental results from Ref. 20; $k_{ET}^{(0)}=\sqrt{2\pi}V^2/\hbar\Gamma$.

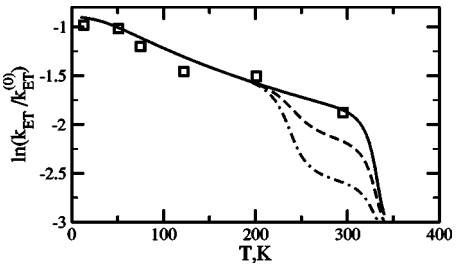

FIG. 8. $k_{ET}/k_{ET}^{(0)}$ vs T at $d\Delta G_e/dT\simeq -1.2$ cm^{-1} K^{-1}. Calculations are carried out at different fraction of water polarization in λ_s [Eq. (38)]: $\theta_W=0$ (solid line), $\theta_W=0.2$ (dashed line), and $\theta_W=0.5$ (dash-dotted line). Squares refer to experimental results (Ref. 20), $k_{ET}^{(0)}=\sqrt{2\pi}V^2/\hbar\Gamma$.

with the density ρ and the distribution function $g(\mathbf{r})$, the corresponding change in the free energy of induction solvation is

$$\Delta G_e=-(\alpha\rho/2)\int[\mathbf{E}_2(\mathbf{r})^2-\mathbf{E}_1(\mathbf{r})^2]g(\mathbf{r})d\mathbf{r}. \tag{40}$$

Assuming that $\mathbf{E}_2$ is much greater in the polar charge-separated state than $\mathbf{E}_1$ in the initial P^* state and adopting a step function for $g(\mathbf{r})$ outside the repulsive cores of the donor and acceptor, one gets

$$\Delta G_e=-2\pi\rho\alpha e^2\left(\frac{1}{R_+}+\frac{1}{R_-}-\frac{2}{R_\pm}\right), \tag{41}$$

where R_+ and R_- are the radii of P^+ and B_L^-, respectively, and $R_\pm$ is the distance between the donor and acceptor; e is the elementary charge. Equation (41) can be further simplified by using the Clausius–Mossotti relation. This yields with $\epsilon_\infty=2.0$:

$$\Delta G_e\simeq-\frac{3e^2}{8}\left(\frac{1}{R_+}+\frac{1}{R_-}-\frac{2}{R_\pm}\right). \tag{42}$$

With $R_+=R_-=5.5$ Å and $R_\pm=11$ Å the above equation gives $\Delta G_e=-1.5$ eV. Further, with the expansion coefficient of the protein matrix 4.7×10^{-4} K^{-1} (Ref. 56) one gets from Eq. (41) $d\Delta G_e/dT\simeq 6$ cm^{-1}/K. A change in the energy gap ΔE_{np}^{Wt} of the order of a few hundred wave numbers over the experimental temperature range of 290 K is therefore quite possible. However, contraction of the protein matrix instead of expansion is necessary to reproduce the experimental temperature dependence of k_{ET}. An increase of protein's density may arise from the difference in expansion coefficients of water and protein. Other sources of the temperature dependence of ΔE_{np} can be anticipated including contraction of the CS dipole ($R_\pm$ distance). A moderate temperature slope of $d\Delta G_e/dT\simeq -1.2$ cm^{-1} K^{-1} turns out to be sufficient to reproduce the observed temperature dependence of the ET rate (Fig. 8) with $\Delta E_{np}^{Wt}=-93$ cm^{-1} obtained from the fit at 295 K in Fig. 7.

It is important to understand how the dynamics of polarization relaxation and reorganization parameters affect dynamical arrest of nuclear solvation. Obviously, the reaction should be sufficiently fast compared to solvent dynamics for dynamical arrest to occur at all temperatures. Figure 8 shows that increasing the contribution of bulk water to the solvent reorganization energy makes solvent dynamics faster leading

to enhancing nuclear solvation on the experimental time scale. The appearance of contributions from nuclear solvation in the reaction thermodynamics then results in a substantial drop of the rate constant at high temperatures. The same effect is achieved by decreasing the electronic donor-acceptor coupling, i.e., by increasing the donor-acceptor separation. With the relaxation times used in the present analysis, the highest temperatures studied experimentally appear almost at the onset of a substantial temperature drop of the ET rate. For the slower rate of charge shift between cytochrome and the primary pair the onset of nuclear solvation falls already into the experimental temperature range.

B. Electron transfer from cytochrome to the primary pair

Primary charge separation is so fast that nuclear solvation is dynamically arrested in the whole temperature range available experimentally. One needs a slower reaction in order to study the occurrence of dynamical arrest. Charge shift from cytochrome *c* to photooxidized primary pair P^+ is a good model reaction since its kinetics is well studied and the reaction rate shows a sharp transition from activated kinetics at high temperatures to no dependence on temperature below 120 K.[57] Early attempts to describe this temperature dependence in terms of changing population of the vibronic states have resulted in unreasonably large vibrational reorganization energies.[58,59] In order to resolve this problem a parallel mechanism was proposed.[60] The cytochrome subunit covalently binds four hemes, two of them are high potential, and two other are low potential. Correspondingly, the parallel mechanism assumes that the low-temperature kinetics is dominated by activationless ET from a low-potential heme, whereas the high-temperature region reflects activated kinetics from the heme closest to P^+. The parallel mechanism is, however, not favored by experiment[33,61,62] which indicates that a sequence of ET steps between hemes, including the uphill transfer[63] between high-potential and low-potential hemes, is a more probable mechanism for supplying the electron to the primary pair.

Recent kinetic studies of high-temperature rates of ET from cytochrome c_2 to the primary donor in Rhodobacter sphaeroides have combined mutagenesis with temperature changes resulting in a more precise assignment of ET parameters.[32] In particular, the high-temperature equilibrium free energy gap, the solvent reorganization energy, and the electronic coupling have been determined from fits of kinetic data to standard ET theories and are listed in Table I. Results of Kaminskaya *et al.*[33] indicate that the equilibrium constant of the reaction between P^+ and the closest high-potential heme is 0.25 below 140 K. From our calculations, nuclear solvation is arrested at these temperatures, and the equilibrium constant is representative of the gap ΔE_{np} which is set equal to zero in the modeling presented below. This makes $\Delta G_n = \Delta G = -0.16$ eV (Ref. 32) at high temperatures. With these parameters, the present theory reproduces well the Arrhenius branch of the photooxidation kinetics of *Chromatium vinosum*[48,57] (Fig. 9). At the transition temperature, the large nuclear reorganization energy characteristic of cytochrome ET (Ref. 64) freezes in and the rate sharply increases. This is not what is seen in experiment. However, the experimental rate reflects the complex kinetics which include both ET between the high-potential heme nearest to P^+ and the chain of transitions between the hemes of the cytochrome unit. The present calculation thus qualitatively agrees with the interpretation of the overall kinetics by Kaminskaya *et al.*,[33] who suggested the establishment of fast equilibrium between P^+ and the closest high-potential heme along with a significant decrease in the concentration of heme's reduced form due to a much slower supply of electrons along the hemes' chain. Note that this interpretation is essentially opposite to that proposed by Ortega and Mathis[62] who suggested that the overall kinetics is determined by slow oxidation of the high-potential heme and its much faster reduction by the adjacent low-potential heme.

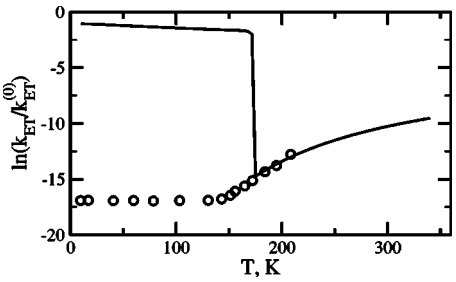

FIG. 9. Rate of charge shift from the high-potential heme of the cytochrome subunit to P^+ vs temperature. Points indicate experimental data for *Chromatium* (Ref. 48). The solid line refers to calculations with parameters from Table I; $k_{\mathrm{ET}}^{(0)} = \sqrt{2\pi} V^2/\hbar\Gamma$.

C. Energy gap law

The calculations of temperature-dependent rates in photosynthetic reaction centers presented here should be viewed as merely an illustration of the consequences of dynamical arrest of nuclear solvation that should be taken into account in the traditional theories of radiationless transitions. The existence of dynamical arrest in these systems still needs to be proved experimentally. Figures 7 and 8 indicate that substantial deviations from the commonly observed flat temperature dependences of fast ET rates become possible when the reaction falls in the nanosecond time range. For these reactively slow reactions, the energy gap law of ET should vary with temperature. Figure 10 shows the energy gap curves calculated with the parameters for primary charge separation taken from Table I at two lower values of the electronic coupling, $V = 3.0\ \mathrm{cm}^{-1}$ and $V = 0.3\ \mathrm{cm}^{-1}$. The upper panel of Fig. 10 shows the slower reaction ($V = 0.3\ \mathrm{cm}^{-1}$). In this case, the maximum of the inverted parabola shifts noticeably to the side of more negative energy gaps when nuclear solvation unfreezes on the time scale of ET. This effect diminishes as ET becomes faster as is shown in the lower panel of Fig. 10 ($V = 3.0\ \mathrm{cm}^{-1}$).

V. DISCUSSION

The current analysis advocates the purely kinetic view of ET in the glass-transition region: lowering the temperature slows down a nuclear mode coupled to ET until the rate of ET becomes comparable to the nuclear relaxation frequency.

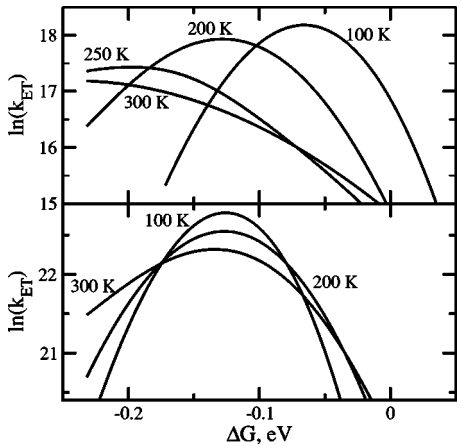

FIG. 10. ET energy gap law at $V=0.3$ cm^{-1} (upper panel) and $V=3$ cm^{-1} (lower panel). The energy gap curves are obtained at various temperatures indicated on the plots. All other parameters are taken from Table I for primary charge separation in *Rhodobacter sphaeroides*.

Further lowering the temperature cuts off the slow nuclear modes from the spectrum of thermal motions activating ET. The result is a pronounced temperature dependence of nuclear reorganization and the activation barrier. This approach is certainly not limited to glass formers and is applicable to any fast ET reaction in a sufficiently sluggish solvent. What makes a glass forming solvent unique in this respect is a very steep change in the structural relaxation time over a very narrow range of temperatures. The resulting fast change of the rate (Fig. 5) may be an attractive feature in cases when high sensitivity to external conditions is desirable, e.g., in the fabrication of molecular devices. For biological systems, on the other hand, high kinetic stability and low sensitivity to temperature changes are significant, and corresponding parts of the photosynthetic system have developed to operate in the dynamically frozen domain.

The microscopic explanation of the dramatic slowdown of structural relaxation is sought in the statistical approach to glass transitions advocating the free energy landscape paradigm.[8] In this approach, the energy of a donor-acceptor complex and the solvent has minima of varying energy as a function of $6N$ coordinate space of N molecules with three translational and three rotational degrees of freedom. Electronic transitions do not span this whole coordinate space and, instead, are sensitive to the single collective reaction coordinate, the energy gap ΔE. It is still an open question whether projecting all the microscopic coordinates on a single reaction coordinate will generate a smooth, single-minimum parabola of the Marcus model or a more rugged landscape. This question is certainly central for a microscopic formulation of the theory.

In view of the fact that the ruggedness of the landscape is directly related to nonlinearity of the solvent relaxation functions,[65] a microscopic formulation of the theory of ET in the region of glass transition will require going beyond the linear response (Gaussian) approximation. The present formulation employs the Gaussian statistics of energy gap fluctuations and thus does not accommodate possible effects of a rugged free energy landscape. The theory by Onuchic and Wolynes (OW) (Ref. 66) seeks to resolve this issue and in fact predicts that the approach to solvent glass transition results in a restriction of the range of allowed values of the solvent reaction coordinate of a given ET reaction. This strongly nonlinear effect then leads to the disappearance of the variance σ_s^2 from the overall variance of energy gaps at some critical temperature, similarly to what follows from the present model. Note, however, that the OW theory does not predict a similar sharp variation of the solvent Stokes shift observed in experiment (Fig. 2).[15] The OW theory was in fact formulated for extremely slow ET reactions assuming that the ET rate is much slower than solvent relaxation, which implies $k_{\mathrm{ET}} \ll 10^{-2}$ s^{-1} at $T \geqslant T_g$.

The common view on the energetics of photosynthetic electron transfer is that the values of the free energy gap and nuclear reorganization energy have been optimized under the evolution pressure to the activationless regime $\Delta G=-(\lambda_s+\lambda_q)$. Several ET reactions in bacterial reaction centers, both charge separation and charge recombination, in fact show a very weak dependence on temperature in a broad temperature range of about 290 K. Although these observations seem to support the view of the activationless character of ET, the broad range of temperatures in which the activationless regime is maintained raises the question of the mechanism of this stability unaffected by solvation despite large dipole moments associated with photosynthetic charge separated states.

In line with the general concept of robust design of photosynthetic reaction centers insensitive to local structural heterogeneity,[67,68] one needs to search for a universal mechanism to stabilize the activationless regime. The concept of dynamical arrest provides such a solution. Slowing down of molecular motions with decreasing temperature is a general property of molecular media. When the rate of ET becomes comparable to the relaxation frequency of a nuclear mode, dynamical arrest leads to a decreasing free energy of nuclear solvation. As a result, the actual values of the nuclear free energy gap and reorganization energy are irrelevant for sufficiently fast ET reactions, ensuring thermal stability of the corresponding rate.

The present formulation of the ET theory supports the view that a close separation of redox centers resulting in fast ET is sufficient for robust kinetics insensitive to temperature variations and details of protein molecular structure.[68] The examination of structures of many natural ET proteins leads to the conclusion that the physiological distances between the edges of redox centers are almost all within 14 Å to ensure that ET is faster than catalytic rates.[69] Longitudinal polarization relaxation adds another time scale. Polarization relaxation should be slow compared to ET in the dynamically arrested regime. The edge to edge distance <6 Å of primary charge separation provides fast enough tunneling to ensure dynamical arrest of nuclear solvation and, consequently, insensitivity to temperature at a relatively low solvent reorganization energy $\lambda_0<0.2$ eV. According to the present calculations, an increase in the donor-acceptor separation would results in a much greater sensitivity to temperature at $T>300$ K unless much slower nuclear dynamics is assumed. It appears, therefore, that a relatively close separation of cofactors is critical for parts of the photosynthetic charge separation chain where preserving the robust and fast

kinetics is important. There is less kinetic pressure on reduction of the primary pair by cytochrome *c* and the edge to edge distance is increased to 12 Å resulting in strongly temperature dependent kinetics at physiological conditions.

ACKNOWLEDGMENTS

The author is grateful to Dr. C. A. Angell, Dr. L. N. Woodbury, and Dr. J. P. Allen for inspiring discussions. Dr. R. Richert has kindly offered his experimental results and assistance in explaining optical spectroscopy in glass-forming solvents. This research was supported by the National Science Foundation (Grant No. CHE-0304694). This is publication No. 593 from the ASU Photosynthesis Center.

[1]R. A. Marcus, Rev. Mod. Phys. **65**, 599 (1993).
[2]L. D. Zusman, Chem. Phys. **49**, 295 (1980).
[3]H. Sumi and R. A. Marcus, J. Chem. Phys. **84**, 4894 (1986).
[4]R. Böhmer and C. A. Angell, in *Disorder Effects on Relaxational Processes*, edited by R. Richert and A. Blumen (Springer, Berlin, 1994).
[5]B. M. Hoffman and M. A. Ratner, Inorg. Chim. Acta **243**, 233 (1996).
[6]R. Richert, J. Phys.: Condens. Matter **14**, R703 (2002).
[7]C. J. F. Böttcher, *Theory of Electric Polarization* (Elsevier, New York, 1973), Vol. 2.
[8]P. G. Debenedetti and F. H. Stillinger, Nature (London) **410**, 259 (2001).
[9]A. A. Ovchinnikov and M. Y. Ovchinnikova, Sov. Phys. JETP **29**, 688 (1969).
[10]S. Mukamel, *Principles of Nonlinear Optical Spectroscopy* (Oxford University Press, New York, 1995).
[11]G. D. Mahan, *Many-Particle Physics* (Plenum, New York, 1990).
[12]W. W. Parson and A. Warshel, Chem. Phys. **296**, 201 (2004).
[13]P. A. Lyle, S. V. Kolaczkowski, and G. J. Small, J. Phys. Chem. **97**, 6924 (1993).
[14]D. V. Matyushov, J. Chem. Phys. **120**, 7532 (2004).
[15]R. Richert, J. Chem. Phys. **113**, 8404 (2000).
[16]R. Richert, Chem. Phys. Lett. **199**, 355 (1992).
[17]D. V. Matyushov, J. Chem. Phys. **122**, 044502 2005).
[18]Y. Tanimura, V. B. P. Leite, and J. N. Onuchic, J. Chem. Phys. **117**, 2172 (2002).
[19]L.-M. Martinez and C. A. Angell, Physica A **314**, 548 (2002).
[20]G. R. Fleming, J. L. Martin, and J. Breton, Nature (London) **333**, 190 (1988).
[21]M. Bixon, J. Jortner, and M. E. Mechel-Beyerle, Chem. Phys. **197**, 389 (1995).
[22]H. Sumi and T. Kakitani, J. Phys. Chem. B **105**, 9603 (2001).
[23]M. Volk, G. Aumeier, T. Langenbacher, R. Feick, A. Ogrodnik, and M.-E. Michel-Beyerle, J. Phys. Chem. B **102**, 735 (1998).
[24]N. J. Cherepy, A. P. Shreve, L. J. Moore, S. Franzen, S. G. Boxer, and R. A. Mathies, J. Phys. Chem. **98**, 6023 (1994).
[25]J. C. Williams, R. G. Alden, H. A. Murchison, J. M. Peloquin, W. W. Woodbury, and J. P. Allen, Biochemistry **31**, 11029 (1992).
[26]Y. Jia, T. J. DiMagno, C.-K. Chan *et al.*, J. Phys. Chem. **97**, 13180 (1993).
[27]H. A. Murchison, R. G. Alden, J. P. Allen, J. M. Peloqin, A. K. W. Taguchi, N. W. Woodbury, and J. C. Williams, Biochemistry **32**, 3498 (1993).
[28]A. L. M. Haffa, S. Lin, E. Katilius, J. C. Williams, A. K. W. Taguchi, J. P. Allen, and N. W. Woodbury, J. Phys. Chem. B **106**, 7376 (2002).
[29]M. Ceccarelli and M. Marchi, J. Phys. Chem. B **107**, 5630 (2003).
[30]W. W. Parson and A. Warshel, J. Phys. Chem. B **108**, 10474 (2004).
[31]G. J. Small, J. M. Hayes, and R. J. Silbey, J. Phys. Chem. **96**, 7499 (1992).
[32]G. Venturoli, F. Drepper, J. C. Williams, J. P. Allen, X. Lin, and P. Mathis, Biophys. J. **74**, 3226 (1998).
[33]O. Kaminskaya, A. A. Konstantinov, and V. A. Shuvalov, Biochim. Biophys. Acta **1016**, 153 (1990).
[34]M. H. Vos, M. R. Jones, C. N. Hunter, J. Breton, J.-C. Lambry, and J.-L. Martin, Biochemistry **33**, 6750 (1994).
[35]C. A. Angell, Annu. Rev. Phys. Chem. **34**, 593 (1983).
[36]G. P. Johari, Phys. Chem. Chem. Phys. **2**, 1567 (2000).
[37]R. S. Smith and B. D. Kay, Nature (London) **398**, 788 (1999).
[38]D. Bertolini, M. Cassettari, and G. Salvetti, J. Chem. Phys. **76**, 3285 (1982).
[39]A. Oleinikova, P. Sasisanker, and H. Weinärtner, J. Phys. Chem. B **108**, 8467 (2004).
[40]G. Barut, P. Pissis, R. Pelster, and G. Nimitz, Phys. Rev. Lett. **80**, 3543 (1998).
[41]T. Simonson and D. Perahia, Faraday Discuss. **103**, 71 (1996).
[42]T. Simonson, Rep. Prog. Phys. **66**, 737 (2003).
[43]P. E. Smith, R. M. Brunne, A. E. Mark, and W. F. van Gunsteren, J. Phys. Chem. **97**, 2009 (1993).
[44]J. W. Pitera, M. Falta, and W. F. van Gunsteren, Biophys. J. **80**, 2546 (2001).
[45]C. L. Brooks and M. Karplus, J. Mol. Biol. **208**, 159 (1989).
[46]J. L. Green, J. Fan, and C. A. Angell, J. Phys. Chem. **98**, 13780 (1994).
[47]A. R. Bizzarri, J. Phys.: Condens. Matter **16**, R83 (2004).
[48]B. J. Hales, Biophys. J. **16**, 471 (1976).
[49]E. Schlodder, K. Falkenberg, M. Gergeleit, and K. Brettel, Biochemistry **37**, 9466 (1998).
[50]M. Vincent, A.-M. Gilles, I. M. L. de la Sierra, P. Briozzo, O. Bârzu, and J. Gallay, J. Phys. Chem. B **104**, 11286 (2000).
[51]S. Lampa-Pastirk and W. F. Beck, J. Phys. Chem. B **108**, 16288 (2004).
[52]X. J. Jordanides, M. J. Lang, X. Song, and G. R. Fleming, J. Phys. Chem. B **103**, 7995 (1999).
[53]P. Changenet-Barret, C. T. Choma, E. F. Gooding, W. F. DeGrado, and R. M. Hochsrasser, J. Phys. Chem. **104**, 9322 (2000).
[54]B. E. Cohen, T. B. McAnaney, E. S. Park, Y. N. Jan, S. G. Boxer, and L. Y. Jan, Science **296**, 1700 (2002).
[55]A. V. Gorelov and V. N. Morozov, Biophys. Chem. **28**, 199 (1987).
[56]C. H. Chang, M. Hayashi, K. K. Liang, R. Chang, and S. H. Lin, J. Phys. Chem. B **105**, 1216 (2001).
[57]D. de Vault and B. Chance, Biophys. J. **6**, 825 (1966).
[58]J. J. Hopfield, Proc. Natl. Acad. Sci. U.S.A. **71**, 3640 (1974).
[59]J. Jortner, J. Chem. Phys. **64**, 4860 (1976).
[60]M. Bixon and J. Jortner, J. Phys. Chem. **90**, 3795 (1986).
[61]T. Kihara and J. A. McCray, Biochim. Biophys. Acta **292**, 297 (1973).
[62]J. M. Ortega and P. Mathis, Biochemistry **32**, 1141 (1993).
[63]I.-P. Chen, P. Mathis, J. Koepke, and H. Michel, Biochemistry **39**, 3592 (2000).
[64]I. Muegge, P. X. Qi, A. J. Wand, Z. T. Chu, and A. Warshel, J. Phys. Chem. B **101**, 825 (1997).
[65]H. Fujimori, H. Fujita, and M. Oguni, Bull. Chem. Soc. Jpn. **68**, 447 (1995).
[66]J. N. Onuchic and P. G. Wolynes, J. Chem. Phys. **98**, 2218 (1993).
[67]C. C. Moser, J. M. Keske, K. Warncke, R. S. Farid, and P. L. Dutton, Nature (London) **335**, 796 (1992).
[68]C. C. Moser, C. C. Page, R. J. Cogdell, J. Barber, C. A. Wraight, and P. L. Dutton, *Advances in Protein Chemistry* (Elsevier, New York, 2003), Vol. 63, p. 71.
[69]C. C. Page, C. C. Moser, X. Chen, and P. L. Dutton, Nature (London) **402**, 47 (1999).